AGU PUBLICATIONS

Water Resources Research

RESEARCH ARTICLE
10.1002/2015WR017412

Key Points:
- Coupled flow-seismic inversion is proposed for fractured media characterization
- Novel seismic inversion provides the structural organization of compliance field
- Inversion with flow data constrains rock-physics model and seismic error model

Correspondence to:
R. Juanes,
juanes@mit.edu

Citation:
Kang, P. K., Y. Zheng, X. Fang, R. Wojcik, D. McLaughlin, S. Brown, M. C. Fehler, D. R. Burns, and R. Juanes (2016), Sequential approach to joint flow-seismic inversion for improved characterization of fractured media, *Water Resour. Res.*, *52*, doi:10.1002/2015WR017412.

Received 17 APR 2015
Accepted 13 JAN 2016
Accepted article online 18 JAN 2016

Sequential approach to joint flow-seismic inversion for improved characterization of fractured media

Peter K. Kang[1,2,3], Yingcai Zheng[2,4], Xinding Fang[2], Rafal Wojcik[1], Dennis McLaughlin[1], Stephen Brown[2], Michael C. Fehler[2], Daniel R. Burns[2], and Ruben Juanes[1,2]

[1]Department of Civil and Environmental Engineering, Massachusetts Institute of Technology, Cambridge, Massachusetts, USA, [2]Earth Resources Laboratory, Department of Earth, Atmospheric and Planetary Sciences, Massachusetts Institute of Technology, Cambridge, Massachusetts, USA, [3]Center for Water Resource Cycle Research, Korea Institute of Science and Technology, Seoul, South Korea, [4]Department of Earth and Atmospheric Sciences, University of Houston, Houston, Texas, USA

Abstract Seismic interpretation of subsurface structures is traditionally performed without any account of flow behavior. Here we present a methodology for characterizing fractured geologic reservoirs by integrating flow and seismic data. The key element of the proposed approach is the identification—within the inversion—of the intimate relation between fracture compliance and fracture transmissivity, which determine the acoustic and flow responses of a fractured reservoir, respectively. Owing to the strong (but highly uncertain) dependence of fracture transmissivity on fracture compliance, the modeled flow response in a fractured reservoir is highly sensitive to the geophysical interpretation. By means of synthetic models, we show that by incorporating flow data (well pressures and tracer breakthrough curves) into the inversion workflow, we can simultaneously reduce the error in the seismic interpretation and improve predictions of the reservoir flow dynamics. While the inversion results are robust with respect to noise in the data for this synthetic example, the applicability of the methodology remains to be tested for more complex synthetic models and field cases.

1. Introduction

Characterizing fractured geologic formations is essential in hydrogeology, exploration geophysics, and petroleum engineering. Fractures often dominate flow and transport behavior in fractured media [*Bear et al.*, 1993], which makes fracture characterization a critical step to the design and risk assessment of nuclear waste disposal [*Pruess et al.*, 1990; *Molinero et al.*, 2002; *Cvetkovic et al.*, 2004; *Martinez-Landa et al.*, 2012], geothermal energy production [*Grant et al.*, 1983], groundwater use [*Duguid and Lee*, 1977; *Kiraly*, 1979, 1987; *Le Borgne et al.*, 2006; *Yadav and Singh*, 2007; *Kang et al.*, 2015a], and induced seismicity [*González et al.*, 2012; *Jha and Juanes*, 2014]. Similarly, much of the current oil and gas reserves worldwide are from reservoirs that are naturally fractured [*Kazemi and Gilman*, 1993]. The relevance of fracture characterization has only increased in recent years with the growth of unconventional resources like shale oil and shale gas [*Curtis*, 2002; *Cueto-Felgueroso and Juanes*, 2013]. Determining the effectiveness and longevity of hydrocarbon production in those environments depends critically on our ability to characterize natural and induced fractures [*Warner et al.*, 2012; *Engelder*, 2012].

Traditionally, seismic interpretation and flow modeling have been performed independently. Both in hydrogeologic applications and the upstream oil and gas industry, reservoir modeling typically follows a unidirectional workflow. From an interpretation of seismic surveys and other geophysical and geological data, a structural reservoir model—with reservoir geometry and faults—is built. Facies data and inference are then used to populate reservoir properties like porosity and permeability on a fine grid, known as a static model (or geomodel). The number of cells in the geomodel is typically too large to perform reservoir flow studies, so a dynamic model is built from either upscaling procedures [e.g., *Durlofsky*, 1991; *Chen et al.*, 2003] or multiscale techniques [e.g., *Arbogast*, 2002; *Jenny et al.*, 2003; *Aarnes*, 2004; *Aarnes et al.*, 2005; *Kippe et al.*, 2008; *Juanes and Dub*, 2008; *Juanes and Tchelepi*, 2008], which solve the global reservoir flow equations on a coarser grid. Rock-physics properties like porosity and permeability, and reservoir dynamics properties like

relative permeability and capillary pressure, are then modified to history-match production data. By then, all feedback to the originating seismic data, and often much of the geologic realism, is lost.

During the past two decades, joint flow-geophysics inversion has received increased attention, especially in the context of hydrogeophysics [e.g., *Hubbard and Rubin*, 2000]. Most joint inversion algorithms can be classified into two categories: (1) those that rely on a close functional relation between geophysical and hydrological parameters [*Rubin et al*., 1992; *Hyndman et al*., 2000; *Linde et al*., 2006; *Irving and Singha*, 2010; *Hinnell et al*., 2010], and (2) those that use zonation, where hydrological and geophysical estimates are assumed to have a similar zonation structure [*Hyndman et al*., 1994; *McKenna and Poeter*, 1995; *Lochbühler et al*., 2013].

Rubin et al. [1992] first proposed a method to estimate a synthetic hydraulic conductivity field by combining sparsely sampled hydrologic data with a seismic velocity model, assuming that an accurate relationship between seismic velocity and hydraulic conductivity is known. *Copty et al*. [1993] took a similar approach to estimate the spatial distribution of permeability, but accounting for errors in the geophysical image. *Hyndman et al*. [2000] used field-scale measurements, rather than a lab-based relation, to estimate seismic slowness and aquifer properties of interest. Building on the work by *Hyndman et al*. [2000], and given the intrinsic limitations of using geophysical models as data due to the imperfect and variable tomographic resolution [*Day-Lewis et al*., 2005], *Linde et al*. [2006] presented a methodology to estimate hydraulic conductivity fields using radar tomograms without assuming that the petrophysical relationships are constant across interpreted velocity zones.

Hyndman et al. [1994] used a split inversion method to extract the geometry of lithologic zones, and successfully estimated the seismic velocity field and the conductivity field by combining seismic and tracer transport data. This approach does not require a strong correlation between geophysical and hydrological parameters, but does rely on the assumption that the zonation of the seismic velocity field and hydraulic conductivity field is identical. Since this approach is not built on a direct relationship between seismic and flow properties, this methodology has limited applicability to complex geologic structures such as fractured media, where it is challenging to define a representative elementary volume (REV).

Seismic interpretation in challenging geologic environments like naturally fractured reservoirs is plagued with uncertainties [*Burns et al*., 2007], which have limited the success of joint interpretation of hydrologic and geophysical data [*Chen et al*., 2006; *Dorn et al*., 2012]. Therefore, there is a pressing need for an approach that combines multiple measurements for characterizing fractured geologic media. In this study, we combine geophysical inversion using the double-beam method (a seismic inversion method tailored to the interpretation of fractured media) with hydrologic data via a rock-physics relation that is assumed stationary within the field.

The goal of our work is twofold: on one hand, to reduce the uncertainty in seismic analysis by incorporating dynamic flow measurements into the seismic interpretation; on the other, to improve the predictive ability of reservoir models by making joint use of seismic and flow data. The basic tenet of our proposed framework is that there is a strong interdependence—but nevertheless not known a priori—between fracture transmissivity (which drives the flow response) and fracture compliance (which drives the seismic response). This connection has long been recognized [*Unger and Mase*, 1993; *Pyrak-Nolte and Morris*, 2000; *Lee and Cho*, 2002], and recent works have pointed to the potential of exploiting that connection [*Vlastos et al*., 2006; *Zhang et al*., 2009; *Brown and Fang*, 2012; *Sayers and den Boer*, 2012; *Petrovitch et al*., 2013]. Here we propose a formal approach to improved characterization of fractured reservoirs, and improved reservoir flow predictions, by making joint use of the seismic and flow responses.

2. Overall Framework

Our approach seeks to combine seismic scattered wavefield data that provide spatial estimates of fracture orientation, spacing, and compliance [*Fang et al*., 2013; *Zheng et al*., 2013] with flow data (pressure and concentration, or saturation) at a number of well locations. The fracture compliance values obtained from seismic data analysis are related to transmissivity through a rock-physics model [*Brown and Fang*, 2012], an approach that has been used in past studies [*Unger and Mase*, 1993; *Pyrak-Nolte and Morris*, 2000; *Petrovitch et al*., 2013]. Both the compliance values obtained from the seismic inversion and the rock-physics model potentially contain substantial uncertainty. By combining the flow data and the inverted compliance field in

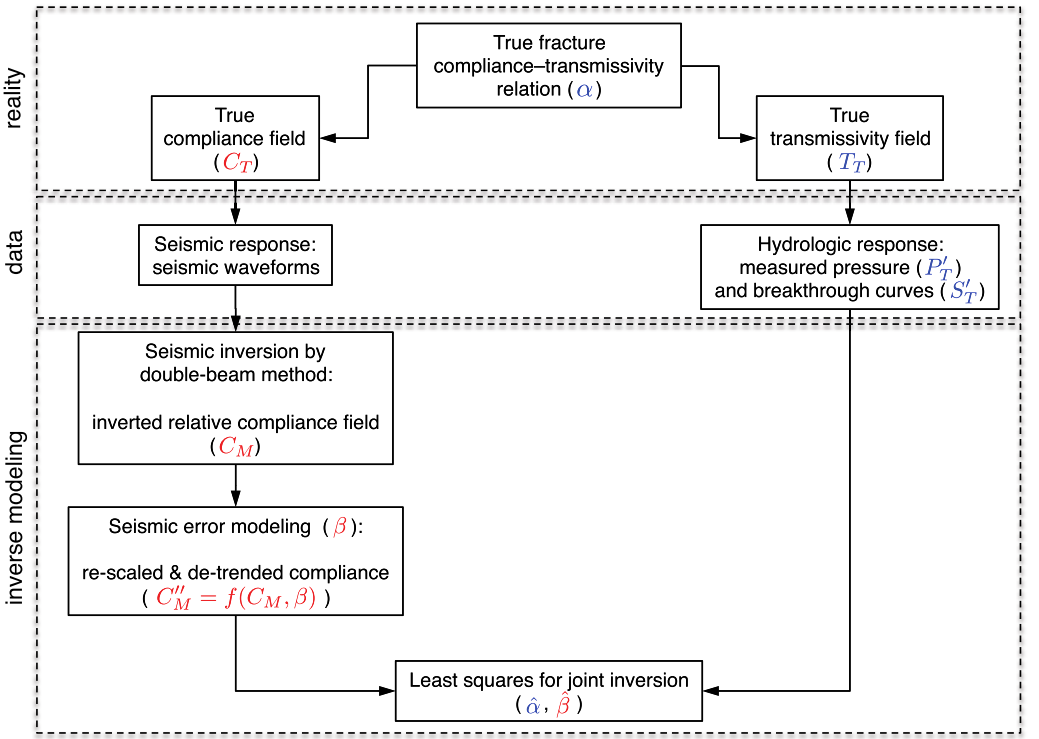

Figure 1. Overall framework for the proposed sequential approach to joint flow-seismic inversion. The key ingredient of our approach is the fracture compliance-to-transmissivity rock-physics relationship that links the seismic response and the flow response. The interpretation of the spatial structure of fracture attributes is performed first using seismic data only, and then hydrologic information is used to scale and detrend compliance values, and to invert for the compliance-transmissivity nonlinear relation. The single joint inversion determines the parameters for both the seismic error model (β) and the compliance-transmissivity rock-physics relationship (α).

a single inversion, we obtain an improved estimation of the subsurface compliance and transmissivity field that reduces the uncertainty and enhances predictions of reservoir flows.

The general workflow is shown in Figure 1. Our proposed framework is rather general and can be applied to field data, although in this paper we restrict our validation to synthetic computer models. We understand the geologic reservoir as being dominated (both in its hydraulic and its seismic responses) by a fracture network. In general, this fracture network can be disordered but have certain geometric statistics (fracture density, length, and orientation), as well as certain elastic compliance statistics for individual fractures (mean, variance, and correlation length). This model of interconnected fractures, which in general is embedded in a reservoir matrix with which it interacts, is the common physical model from which seismic and flow responses are determined. The key ingredient of our approach is the fracture compliance-to-transmissivity relationship, which links the seismic response to the flow response.

The true fracture compliance field (C_T) and true fracture transmissivity field (T_T) are related via a predefined *rock-physics model*, $T_T = f(C_T, \alpha)$, where α denotes a set of parameters governing the functional relation between fracture compliance and transmissivity. The strong dependence between fracture compliance and transmissivity can be ascertained from simulations of fluid flow and elastic deformation on rough-walled fractures (Figure 2a). The objective is then to infer the true compliance field and compliance-transmissivity relationship by a procedure that unifies seismic and flow modeling.

2.1. Seismic Inversion and Error Modeling

We first run a forward seismic simulation on the true compliance field (C_T) to generate the detailed wavefield [*Schoenberg*, 1980; *Coates and Schoenberg*, 1995; *Fang et al.*, 2013]. The seismic response is affected by the underlying fracture mechanics parameters, such as fracture orientation, spacing, and compliance. In a field application, this step is equivalent to recording seismic wavefields using surface geophones.

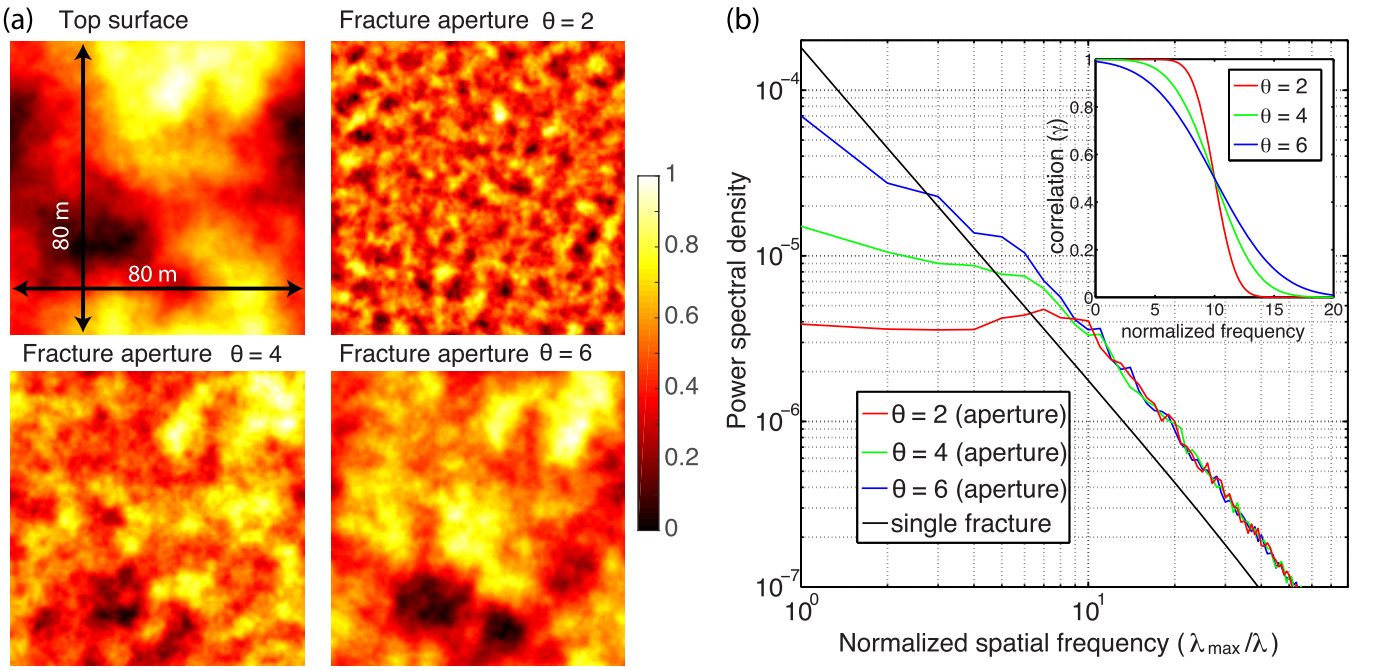

Figure 2. (a) Top fracture surface, where the horizontal and vertical length is $L = 80$ m, and fracture aperture maps (void space between the top and bottom surface) for three different values of the phase-change correlation parameter θ (see Appendix A). For this work, we choose $D_f = 2.5$ for fractal dimension, $k_c = 10$ for the normalized critical frequency, and $\sigma_f = 0.02$ m for the standard deviation of surface heights. Shown are the aperture values normalized with respect to the maximum value. (b) Power spectral density for three different values of θ. The change in power spectral density is smoother as θ increases. Inset: correlation function γ for different θ values.

We take these wavefields and estimate the spatial map of seismic compliance (C_M) by means of the double-beam seismic inversion method [*Zheng et al.*, 2013]. In general, the method can be used to determine the orientation of sets of fractures, fracture density, and fracture compliance as a function of space (see Appendix B for details). The double-beam method, however, only provides relative compliance values (that is, on a different scale than the true compliance values), and the error in the estimated compliance field, $e_c = C_T - C_M$, often exhibits a strong spatial correlation with the actual compliance field C_T; something that points to the need to model (rescale and detrend) this error to reduce such dependence. Methodologically, this implies a transformation $C_M \rightarrow C_M^{'}$ (rescaled) $\rightarrow C_M^{''}$ (detrended) such that the error in the transformed variable, $e_c^{''} = C_T - C_M^{''}$, is only weakly dependent on the underlying (and unknown) true compliance field. This error-modeling introduces a set of parameters, β, governing the scaling and detrending of the estimated fracture compliance field.

2.2. Flow Modeling

The flow response relies on the compliance-to-transmissivity relation, from which we generate the true fracture transmissivity field, T_T. We simulate fluid flow and solute transport on this transmissivity field, from which we extract a dynamic record of pressure (P_T) and breakthrough curves of the solute (S_T) at a discrete set of locations that represent well measurements. These records are subject to measurement errors, and therefore we denote the accessible, measured quantities as $P_T^{'}$ and $S_T^{'}$, respectively. The set of parameters α generating this response via the compliance-to transmissivity relation, $T_T = f(C_T, \alpha)$, are of course unknown. We run the flow model ($\mathcal{G}_P$) and transport model ($\mathcal{G}_S$) on estimates $\hat{T}_T(\hat{\alpha}, \hat{\beta})$ to obtain modeled responses $\hat{P}_T$ and $\hat{S}_T$. The sets of parameters $\hat{\alpha}$ (parameters determining the rock-physics model) and $\hat{\beta}$ (parameters determining the error model for inverted compliance) are then estimated by minimizing the error between the measured $(P_T^{'}, S_T^{'})$ and modeled $(\hat{P}_T, \hat{S}_T)$ flow response. Given that only a handful of parameters need to be estimated, this is an overdetermined problem [*Menke*, 2012]. While sophisticated estimation and inversion procedures exist, our work employs a simple weighted least squares minimization procedure:

$$\min_{\hat{\alpha},\hat{\beta}} \left[\sum w_P \left(P_T^{'} - \mathcal{G}_P(\hat{T}_T(\hat{\alpha}, \hat{\beta})) \right)^2 + \sum w_S \left(S_T^{'} - \mathcal{G}_S(\hat{T}_T(\hat{\alpha}, \hat{\beta})) \right)^2 \right]. \quad (1)$$

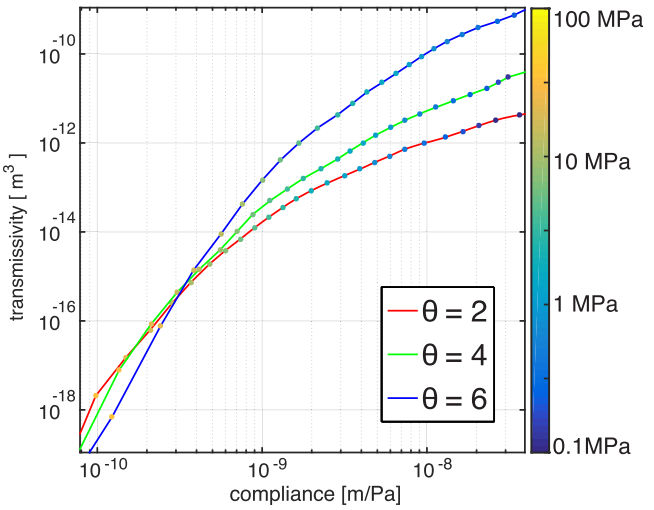

Figure 3. Functional relation between fracture compliance [m Pa^{-1}] and fracture transmissivity [m^2 s^{-1}], obtained from simulation of fluid flow and elastic deformation on rough-walled fractures for three different θ values. We parameterize the functional relation with a set of parameters α using the polynomial fit to the data in log-log space: $\log(T) = \alpha_1 \log(C_T)^2 + \alpha_2 \log(C_T) + \alpha_3$. The colors of solid circles indicate the normal stress on the fracture at each point of the compliance-transmissivity curves: the normal stress for compliance values between 10^{-10} and 10^{-9} m Pa^{-1} is around 30 MPa.

The weighting factors w_P and w_S normalize the contribution of different data sets: pressure values and breakthrough curves at observation wells. An obvious challenge is the determination of these weighting factors. If there is no a priori information on the accuracy of each data set, we make two a priori assumptions. First, we assume that measurement errors are independent. Second, we assume the measurement errors are proportional to the magnitude of the measured values to normalize the contribution of two different data sets [*Kool and Parker*, 1988]. This is a simple way to account for the different units and different measuring instruments used in the two data sets. Therefore, we take the second moment of the mean pressure measurement and the mean breakthrough mass fraction measurement as the weighting factors, w_P [Pa^{-2}] and w_S [−], respectively.

2.3. Rock-Physics Model

A rock-physics model links seismic observables into reservoir properties. In this study, a rock-physics model is a physical relation between fracture compliance and fracture transmissivity, which is needed to convert seismic scattering measurements into data useful for hydrologic modeling. To study the relation between fracture compliance and fracture transmissivity, we perform simulations of fluid flow and elastic deformation on a rough-walled fracture (Figure 2). We construct a rock-physics model in three independent steps: (1) we generate rough fracture surfaces; (2) we solve the elastic deformation problem on the rough-walled fractures under normal stress; and (3) we solve the flow problem through the stressed (deformed) rough-walled fractures. These steps allow us to construct a regression-based rock-physics model derived from data calculated using the mechanistic model (Figure 3).

We first extend the methodology of *Brown* [1995] to better represent the correlated structure of fracture roughness, and implement the method of *Andrews* [1988] and *Unger and Mase* [1993] to run efficient simulations of the elastic contact problem. Finally, we solve the flow problem on the deformed rough-walled fractures by assuming a parallel-flow approximation where the local aperture value represents the fracture width [*Moreno et al.*, 1988; *Moreno and Neretnieks*, 1993]. We obtain the effective fracture compliance value by solving the elastic contact problem and the corresponding effective transmissivity value by solving the flow problem. The detailed procedure for each step can be found in Appendix A.

We generate the rock-physics model by plotting the obtained fracture transmissivity values with respect to the fracture compliance values. We typically obtain concave shapes for the functional relation for various combination of parameters (Figure 3). However, different shapes can emerge depending on the rock type [*Pyrak-Nolte and Morris*, 2000].

3. Synthetic Example

We test our coupled flow-seismic inversion framework on discrete fracture networks consisting of two sets of parallel, equidistant, connected fractures oriented at an angle of 0° and 90° with respect to the *x* axis (Figure 4). We assume a layered Earth's model, where one of the layers is a fractured reservoir layer (see Appendix B for a detailed description). For simplicity, the fracture planes in this layer are vertical and bounded by the thickness of the reservoir layer. The fracture spacing is uniform and equal to 80 m. On average, the value

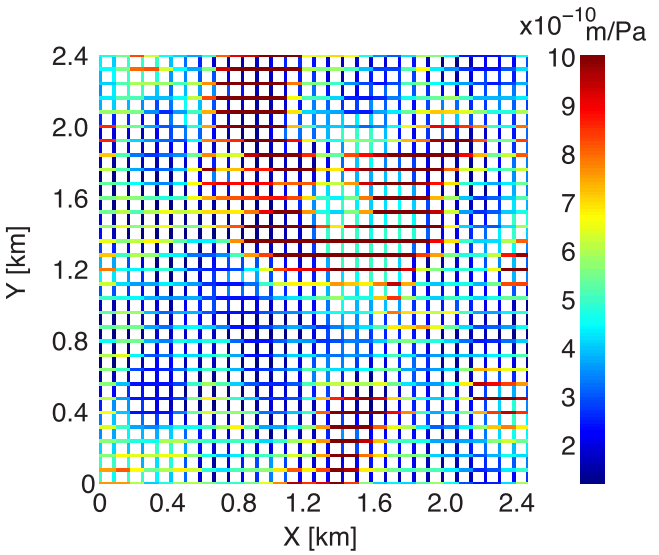

Figure 4. True compliance field (C_T) of the orthogonal discrete fracture networks that we study. Each link has length equal to 80 m and has a compliance value between 10^{-10} and 10^{-9} m Pa^{-1}.

of x directional fracture compliance is 2 times larger than the y directional compliance. Our compliance values vary between 10^{-10} and 10^{-9} m Pa^{-1}, which are in the range of realistic values at the field scale [*Worthington and Lubbe*, 2007; *Bakku et al.*, 2013]. We construct a spatially correlated compliance field that follows a lognormal distribution with an exponential autocorrelation function in space (Figure 4). The fracture compliance field (C_T) is related to the fracture transmissivity field (T_T) via the rock-physics model described in the previous section.

3.1. Seismic Inversion on Orthogonal Discrete Fracture Networks

We run seismic forward modeling by simulating seismic shot gathers using a 3-D staggered grid finite difference method [*Coates and Schoenberg*, 1995; *Willis et al.*, 2006; *Fang et al.*, 2013]. Seismic signals contain two types of errors or noise. The first one is random noise. This type of error (noise) can be greatly reduced in seismic stacking, so it is usually not a big concern. The second type is the signal-generated noise. This kind of noise is much more challenging, because it can be misidentified as signal. In our synthetic example, the fractured reservoir is placed in a geological layered structure. The strata boundaries introduce this signal-generated noise, which is therefore included in the seismic data set. An important feature of our fracture-imaging algorithm is that those reflections from geologic layers are naturally separated and discarded.

For seismic inversion, we apply the double-beam method [*Zheng et al.*, 2013] to estimate the modeled seismic compliance field C_M. The method exploits multiply scattered waves, which contain fracture orientation and spacing information, and the amplitude of these waves, which contains compliance information. To interpret the fracture-scattered signals, we make use of the interference of two focusing Gaussian beams emitted from the surface source and receiver arrays. A more detailed explanation of the double-beam method is given in Appendix B. The double-beam method can in general estimate fracture density and orientation, and these attributes are indeed estimated accurately for the synthetic example (see Appendix B). For the flow-seismic inversion in the synthetic example, however, we then take fracture spacing and fracture orientations as known, such that only the compliance values, and not the geometry of the fracture network, need to be updated.

3.2. Error Model for the Inverted Compliance Field

By analyzing the inverted compliance field, C_M, obtained from the double-beam method, we find that the compliance estimate has to be rescaled and detrended. This is because the double-beam method measures the fracture-scattered seismic wave (beam) amplitude which can be related to the fracture compliance. As such, it provides a map for the relative fracture compliance values as a function of space.

First, C_M has a different scale than C_T and must be rescaled (Figures 5a and 5b). Therefore, we introduce a rescaling factor, β_0, where $C'_M=\beta_0 C_M$, such that $\langle C'_M\rangle=\langle C_T\rangle$. By plotting the rescaled error, $e'_c=C_T-C'_M$, with respect to the centered true compliance value, we observe that the rescaled error is highly correlated with C_T itself (Figure 5c). From the point of view of estimation, this is undesirable because it would require a priori knowledge of the true compliance field. Thus, we introduce an error model that effectively detrends the modeled response and weakens its dependence on the true compliance field. Our error correction model is motivated by the scatter plot between $C_T-C'_M$ and $C_T-\langle C'_M\rangle$, which shows a near-linear trend (Figure 5d). Thus, we propose the linear error model $e'_c \equiv C_T-C'_M=\eta(C_T-\langle C'_M\rangle)+\epsilon$, where η is a parameter to be

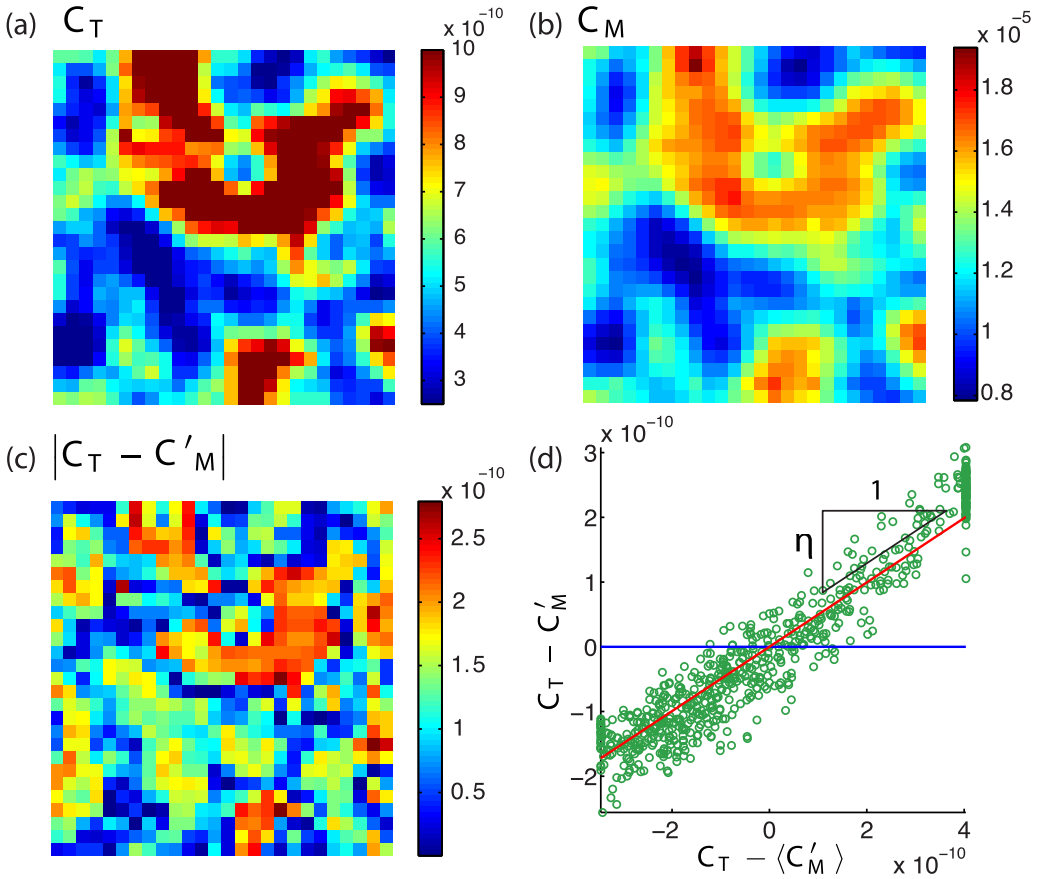

Figure 5. (a) True compliance field for the orthogonal discrete fracture network, interpolated to show the smoothed compliance field (C_T). (b) Inverted compliance field from the double-beam seismic analysis (C_M). Note that the inverted compliance field has to be rescaled to have the same mean as the true compliance field. (c) Difference between true compliance field (C_T) and the rescaled seismic-interpreted compliance field (C'_M). We find that there is strong correlation between the error ($e'_c = C_T - C'_M$) and the true compliance field (C_T), showing the need for detrending. (d) Error (e'_c) as a function of the centered compliance ($C_T - \langle C'_M \rangle$): we observe that C'_M is compressed compared to C_T, and there is a linear relation between the error and the centered compliance.

estimated, and ϵ is a random spatial variable that exhibits a much lower correlation with C_T. From these observations, and reorganizing, $(1-\eta)C_T = (1-\eta)\beta_0 C_M + \beta_0\eta(C_M - \langle C_M \rangle) + \epsilon$. Therefore, we define $C''_M = \beta_0[C_M + \beta_1(C_M - \langle C_M \rangle)]$ with $\beta_1 = \eta/(1-\eta) > 0$ but unknown, and $e''_c = C_T - C''_M$, which we model as an independent random function. Now our attempt is to estimate the parameters of both the error model and rock-physics model using flow and transport information. This is possible because the fracture compliance field and transmissivity field are linked via the rock-physics model.

3.3. Fracture Compliance-Transmissivity Relation

In this study, we assume the existence of a space-independent rock-physics model and we take the compliance-transmissivity relation shown in Figure 3. To test the effectiveness of our inversion framework, we also investigated three different types of functional relation between fracture compliance and fracture transmissivity (linear, convex, and concave) and confirmed that the framework is equally robust.

3.4. Flow and Transport Through Fracture Networks

We study a simple but realistic flow setting, which can be modeled with a no-flow condition at the boundaries of the fracture network, and fixed pressure values at the single injection well (injection well located at the lower-right corner for training scenario 1, the left center for training scenario 2 and at the lower-left corner for the prediction scenario) and pumping well (pumping well located at the upper-left corner for training scenario 1, the right center for training scenario 2 and at the upper-right corner for the prediction scenario) (Figure 6).

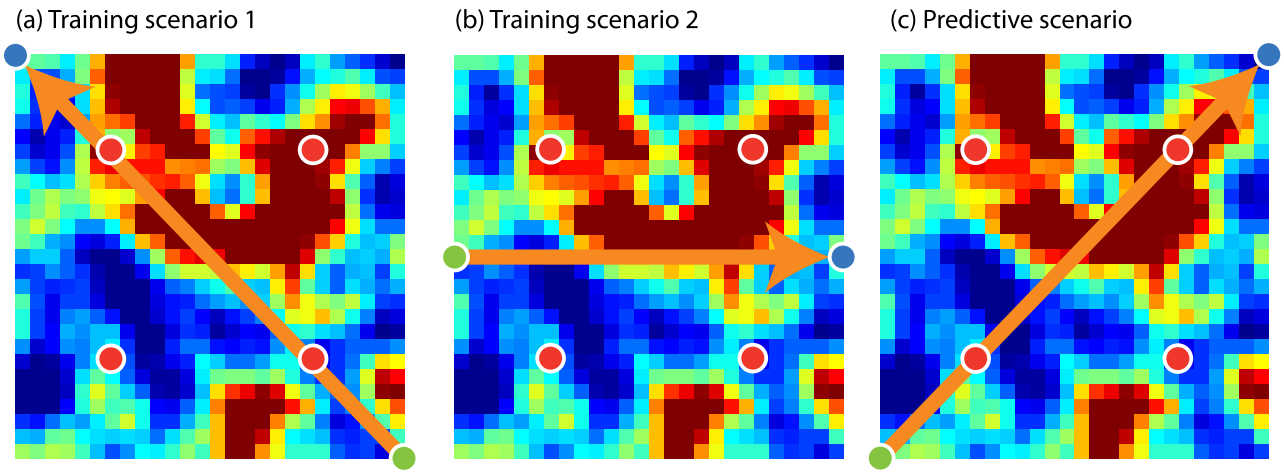

Figure 6. (a) Training flow scenario 1 used in the parameter estimation. Quarter five-spot flow geometry with a single injection well (green circle) and a single pumping well (blue circle). There are four observation wells (red circles) that measure borehole pressure. (b) Training flow scenario 2 used in estimation. A single injection well (green circle) at the left-center and a single pumping well (blue circle) at the right-center. (c) Prediction flow scenario, used to test the predictive ability of the estimated fracture transmissivity field. Quarter five-spot flow geometry along the diagonal direction opposite to that of flow scenario 1. This prediction scenario is not used in the estimation step.

In this synthetic example, we do not consider flow in the matrix. We simulate flow through the fracture network by assuming Poiseuille's law along each fracture, such that the flow rate Q_{ij} between nodes i and j is given by (see Appendix A)

$$Q_{ij} = \frac{T_{ij} W}{\mu} \frac{P_i - P_j}{L}, \tag{2}$$

where P_i and P_j are the fluid pressure values at nodes i and j, L is the distance between nodes (constant in our simple fracture network), W is the width of the fracture in the direction perpendicular to flow (assumed constant), μ is the fluid dynamic viscosity (also assumed constant), and T_{ij} is the compliance-dependent fracture transmissivity. Imposing mass conservation at each node i, and assuming incompressible flow, $\sum_j Q_{ij} = 0$, leads to a linear system of equations, which is solved for the pressure values simultaneously at all the nodes.

Once the flow rates in the fractures are known, we simulate transport of a passive tracer by particle tracking. We neglect diffusion, and thus particles are advected with the flow velocity between nodes. We assume complete mixing at the nodes. Thus, the link through which the particle exits a node is chosen randomly with flux-weighted probability [*Moreno et al.*, 1988; *Moreno and Neretnieks*, 1993; *Kang et al.*, 2011, 2015b]. This particle-tracking simulation allows us to compute the breakthrough curves (first-passage time distribution) of the injected tracer at the pumping well.

3.5. Unifying Flow Measurements and Seismic Interpretation by Least Squares

To characterize the fracture compliance field, we unify flow measurements and seismic interpretation. Pressure values and breakthrough curves at wells are used as flow measurements, which can be obtained by solving the pressure and transport equations on the true transmissivity field (T_T). The objective is to find the set of parameters, α (which characterizes the functional relation between T_T and C_T, Figure 3) and β (which characterizes the error model of the inverted compliance field, Figure 5d), by minimizing the objective function in equation (1), that is, the sum of the weighted squares of the difference between measured and simulated pressure (P_M and $\hat{P}_T$) and the difference between measured and simulated tracer breakthrough curves (S_M and $\hat{S}_T$) from the rescaled and detrended seismically interpreted compliance field (C''_M). As input for our weighted least squares minimization procedure, we used two flow scenarios (training scenarios 1 and 2), each with four pressure observation wells and one tracer breakthrough curve at the extraction well (Figure 6).

A global optimization algorithm is applied to find a set of parameters (α, β) that minimize the objective function. Specifically, we used pattern search [*Hooke and Jeeves*, 1961] and particle swarm [*Eberhart and Kennedy*, 1995; *Shi and Eberhart*, 1998] algorithms, which do not require the gradient of the objective

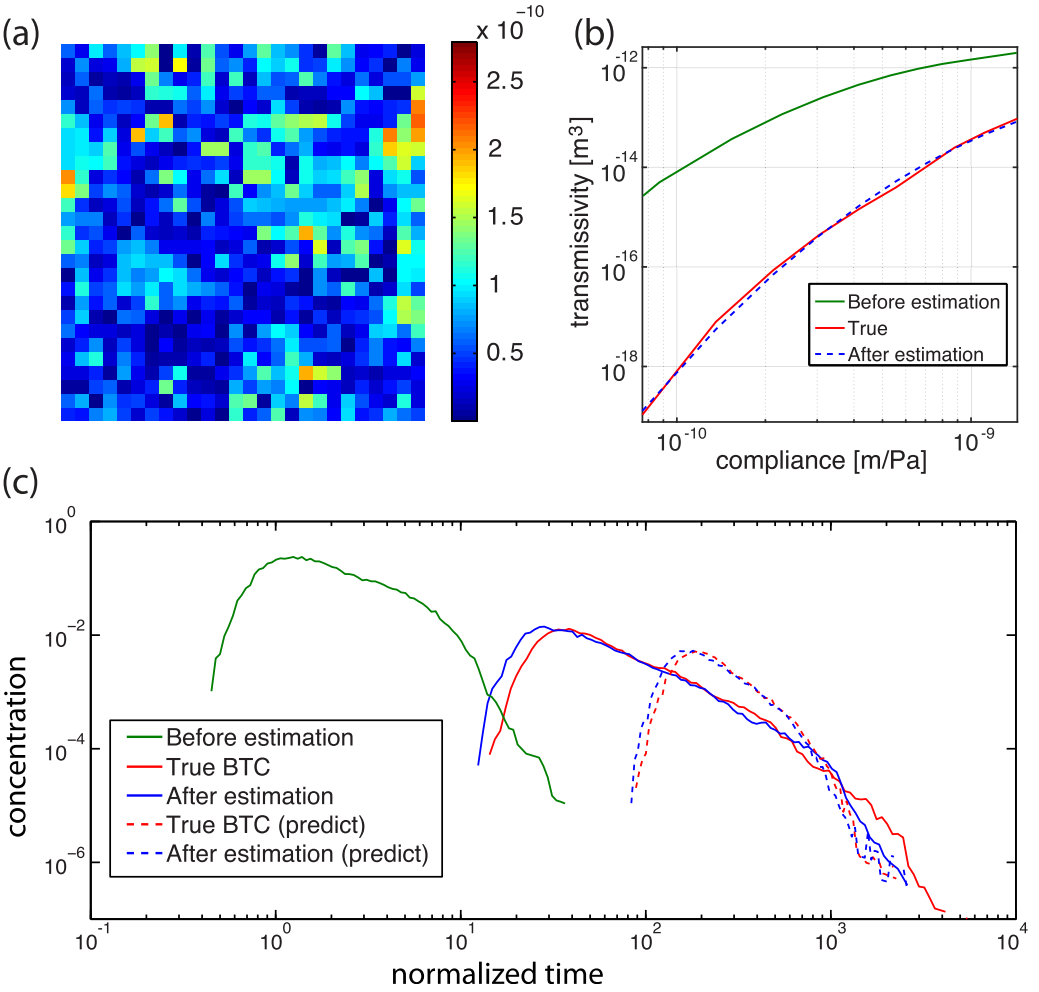

Figure 7. (a) Difference between the true compliance field (C_T) and the corrected seismically interpreted compliance field (C''_M), which shows that the corrected compliance error ($e''_c = C_T - C''_M$) is small and virtually independent of the true compliance field C_T. (b) The estimated compliance-transmissivity relationship from our coupled flow-seismic inversion (blue line) accurately captures the true compliance-transmissivity relationship (red line), even though the initial input for our least squares procedure is grossly inaccurate (green line). (c) Tracer breakthrough curves before (green solid line) and after inversion (blue solid line) compared with the true response (red solid line). The dashed lines show the performance of the model in *predictive mode*, in which the model is used after inversion to predict the flow response for a different well configuration (prediction flow scenario).

function during the minimization. We found that the pattern search algorithm was sensitive to the initial guess of target parameters, whereas the particle swarm algorithm provided more stable and accurate estimates of the target parameters. In our inversions, we found that launching 50 "particles" was sufficient to obtain a robust minimization of the objective function in equation (1).

As can be seen in Figure 5, the inverted compliance field (C_M) obtained from the double-beam seismic method provides excellent information on the structural organization of the compliance field, but not necessarily on its magnitude. Since flow data are sensitive to both absolute values and structural organization of the compliance field, our sequential approach to joint inversion allows us to unify flow measurements and seismic interpretation to estimate the true compliance field. To test the predictive ability of our estimated compliance field, we use for prediction purposes a flow scenario that is not used in the estimation step (Figure 6c).

3.6. Sequential Coupled Flow-Seismic Inversion Results

We find that the fracture field can be accurately characterized from the sequential coupled inversion of seismic and flow data (Figure 7).

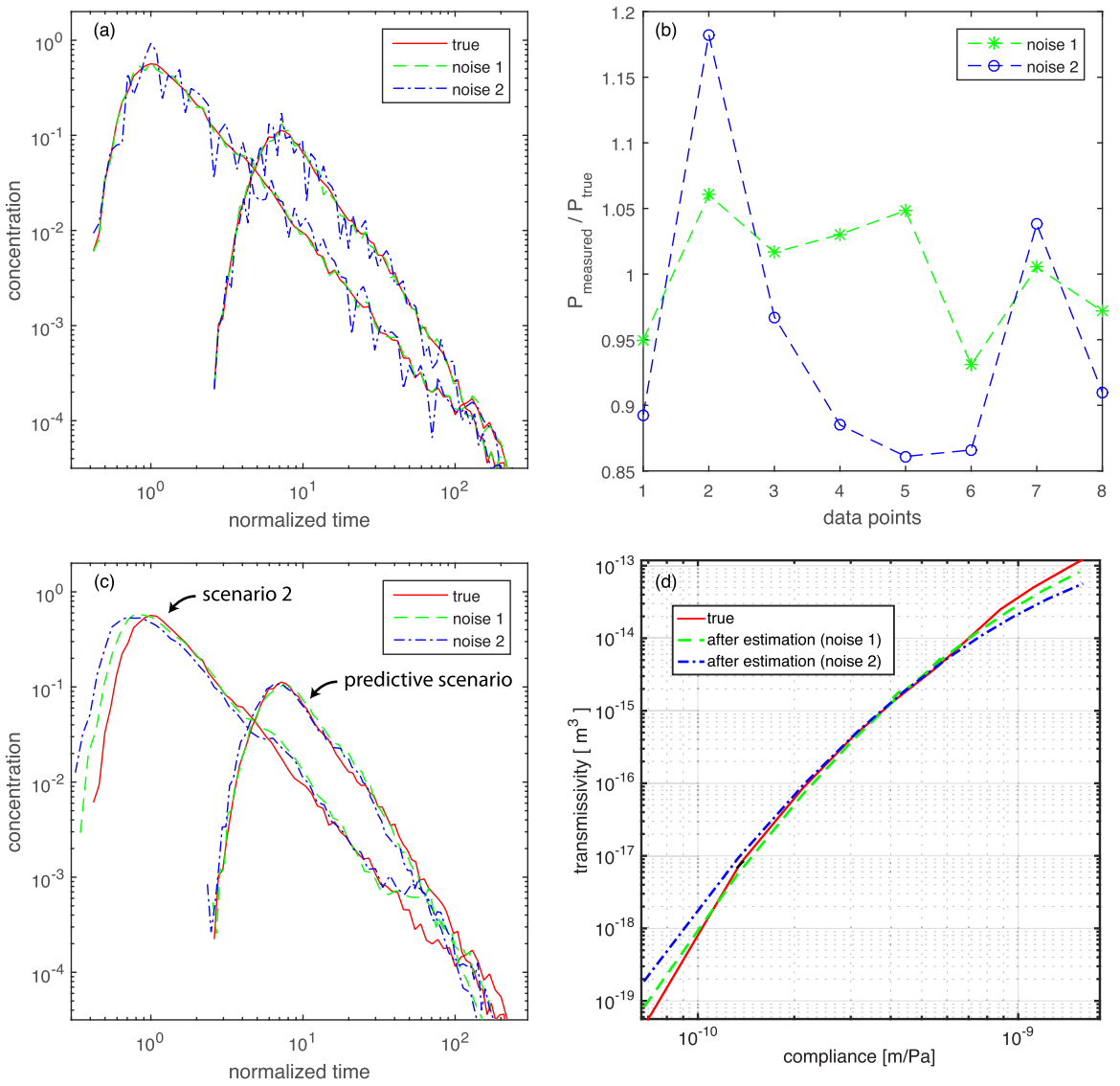

Figure 8. Impact of noise in the hydrologic data on inversion results. (a) Breakthrough curves for training scenario 2 with different levels of noise. (b) Corresponding pressure measurements at the wells in training scenarios 1 and 2. Shown are the ratios of the measured pressure to the true pressure. (c) Estimated and predicted breakthrough curves for the two different noise levels. (d) Comparison between the true fracture compliance-transmissivity relation and the outcome of the inversion methodology for the two different noise levels.

The first indication of the validity of the approach is the error structure in the estimated compliance field (Figure 7a). The error in the estimated compliance, $e_c''=C_T-C_M''$, is small in magnitude and exhibits significantly decreased correlation with the true compliance field (compare Figures 5c and 7a). The mean error for $|C_T-C_M''|$ showed a factor-of-two reduction compared with $|C_T-C_M'|$, and the correlation coefficient between C_T and $|C_T-C_M''|$ showed a factor-of-two reduction compared with the correlation coefficient between C_T and $|C_T-C_M'|$. This behavior points to the importance of the rescaling and detrending steps in obtaining an effective error model for the inverted compliance field. Since the fracture compliance and transmissivity values are linked via the rock-physics model, the accurate estimation of the fracture compliance field and the rock-physics model (Figures 7a and 7b) implies the accurate estimation of the transmissivity field.

The second indication is the remarkable accuracy with which the functional relationship between compliance and fracture transmissivity was estimated (Figure 7b), despite the paucity of dynamic flow data used. The improvements in the estimates of the compliance field and the compliance-to-transmissivity relation

lead to substantial improvements in the ability of the model to *predict* the breakthrough curve for a different flow scenario (prediction flow scenario, Figure 6c) in which the injection and pumping wells are located on a diametrically opposite pattern (Figure 7c).

3.7. Impact of Noisy Hydrologic Data

The accuracy and robustness of the inversion are partly due to the idealized setup of the synthetic test case. In this section, we test the degree to which the inversion results for our synthetic example are sensitive to the presence of noise in the hydrologic data. We incorporated measurement errors by adding white Gaussian noise to both the tracer breakthrough curve and the pressure measurements. We considered two noise levels: (1) a mild noise level, with standard deviation of $S_T/50$ and $P_T/50$ for the breakthrough curves and pressure measurements, respectively; and (2) a strong noise level, with corresponding standard deviations of $S_T/10$ and $P_T/10$.

In Figure 8, we show the results of the inversion for training scenario 2, and the model predictions for the predictive scenario, under different noise levels: no noise, mild noise, and strong noise. It is apparent that even for strong noise levels in tracer breakthrough data (Figure 8a) and pressure data (Figure 8b), the proposed methodology produces excellent predictions of tracer concentration at the extraction well (Figure 8c), and robust estimates of the compliance-transmissivity relation (Figure 8d). Despite the many simplifications introduced in the synthetic example that we study, these results illustrate the robustness of the proposed methodology to the presence of errors that typically pollute hydrologic data in real field cases.

4. Discussion and Conclusions

We have presented a new sequential framework for the coupled inversion of seismic and flow data, for improved characterization of fractured geologic media. The key ingredient of our approach is the recognition that the seismic response and the flow response are linked through a fracture compliance-to-transmissivity rock-physics relationship. We show that seismic and flow data are complementary, where seismic modeling provides the structural organization (fracture orientation and fracture spacing) and relative values of the compliance field, and flow data provide information to rescale and detrend the inverted compliance field. Our methodology is rather general, and was designed to be applicable to real field data, where the true compliance field is unknown, the compliance-to-transmissivity relationship is uncertain, and the flow data are limited. Here we have illustrated the potential of the framework through synthetic computer models of fractured reservoirs. We have shown that integrating seismic interpretation (through the double-beam method [*Zheng et al*., 2013]) with flow modeling leads not only to robust parameter estimation, but also to reservoir flow models that are more predictive.

Although our sequential coupled flow-seismic inversion framework worked well for our test cases, the generality of our methodology has to be investigated further. For example, although real geologic reservoirs often display fracture sets with preferential orientation, fracture length, direction, and spacing are typically random variables, leading to more complex fracture networks. In addition, different rock types and lithologies are characterized by different rock-physics models, which would require the estimation of multiple compliance-transmissivity relations, according to a zonation of the medium by rock type. This added complexity may require, in turn, the implementation of more sophisticated estimation algorithms or data assimilation techniques.

Appendix A: Constructing the Rock-Physics Model

In this appendix, we describe the construction of the rock-physics model in detail.

A1. Model of Rough-Walled Fractures

We construct synthetic rough-walled fractures using the spectral synthesis method (Figure 2a) [*Brown and Scholz*, 1985; *Power and Tullis*, 1991; *Glover et al*., 1998]. From spectral analysis, we decompose each surface of the fracture into two components: a power spectral density function and a phase spectrum. The power spectral density of a real fracture surface exhibits power law decay as a function of wave number k (inverse of wavelength λ), where the exponent is determined by the fractal dimension D_f of the fracture surface [*Brown and Scholz*, 1985; *Goff*, 1990; *Power and Tullis*, 1991; *Brown*, 1995]. The phase spectrum, in contrast, is

often observed to be a near-random process independent of frequency (white noise). Further, experimental observations show that the top and bottom surfaces are highly correlated for long wavelengths but poorly correlated for short wavelengths [*Brown*, 1995; *Glover et al*., 1998]. To incorporate this observation into the numerical, synthetic, rough surface generator, *Brown* [1995] introduced a critical wavelength λ_c, such that the two surfaces are perfectly matched above the critical wavelength and completely independent below it. However, the sharp transition from perfectly correlated to uncorrelated phase at a critical wavelength introduces a sharp discontinuity in the power spectral density. *Glover et al*. [1998] extended Brown's method to allow the surfaces to be matched at long wavelengths and gradually mismatched as the wavelength decreases. However, *Glover et al*. [1998] still assumed zero correlation between the two surfaces below the critical wavelength and the way they generate partially correlated phases above the critical wavelength leads to different variance between the phases of top and bottom surfaces.

Therefore, we propose an extension to the methods of *Brown* [1995] and *Glover et al*. [1998], which allows for a gradual change in correlation as a function of wavelength λ, and preserves the variance between phases of the top and bottom surfaces. Other approaches have been proposed by, e.g., *Ogilvie et al*. [2006] [*Walsh et al*., 2008]. First, we define a critical wavelength, $\lambda_c = 1/k_c$, where the correlation between the top and bottom surface is 0.5. Second, we define the phase correlation function γ of the phases between the top and bottom surfaces as a function of frequency, $k = 1/\lambda$, as follows: $\gamma = \frac{1}{2}[1+\mathrm{erf}(-(k-k_c)/\theta)]$, where θ is a model parameter. The correlation gradually decreases from perfect correlation ($\gamma = 1$) to no correlation ($\gamma = 0$) as the spatial frequency increases (Figure 2b, inset). As defined, $\gamma = 0.5$ at $k = k_c$, and θ determines the rate of change in correlation. The transition from high to low correlation is sharper as θ decreases (Figure 2b, inset).

To construct top and bottom fracture surfaces that follow the correlation structure γ, we assign random phases R_1 for the top surface and generate phases R_2 for the bottom surface such that R_2 have correlation γ with R_1. To assign R_2, we mix two random variables (R_1, R_3) to obtain a new random variable (R_2) such that R_2 and R_1 have correlation γ as follows: $R_2 = \gamma R_1 + \sqrt{1-\gamma^2}R_3$ [*Gabriel and Colburn*, 1981]. Once the phases have been set, we generate the two surfaces by performing an inverse Fourier transform of the combined power and phase spectra. After the two surfaces are generated, we define the standard deviation of surface heights (σ_f) and the mean distance ($\bar{b}$) between top and bottom surfaces. Figure 2a shows the top fracture surface and fracture aperture maps for three different values of θ with fixed $\bar{b}$ that gives a minimum distance between top and bottom surfaces equal to 0 (no penetration).

In summary, we generate the aperture field of a rough-walled fracture with four parameters: the fractal dimension (D_f) that defines the slope of the power spectral density, the standard deviation of the fracture profile (σ_f) that determines the intercept of the power spectral density, the critical wavelength (λ_c), and the rate of change in phase correlation (θ).

A2. Estimation of Fracture Compliance

From the generated fracture aperture map, we obtain the effective compliance via an elastic deformation simulation on the synthetic rough surface, subject to confining stress. Both multilevel multisummation and fast Fourier transform (FFT) have been applied to solve rough contact problems [*Unger and Mase*, 1993; *Nogi and Kato*, 1997; *Polonsky and Keer*, 1999]. We have applied FFT to solve the contact problem, as explained in detail in *Andrews* [1988] and *Unger and Mase* [1993]. We only describe the procedure briefly here. We consider only normal stresses at the contact, and assume that the medium is linearly elastic. As the mean distance $\bar{b}$ between the top and bottom surfaces decreases, a region of interpenetration between the top and bottom surfaces emerges. We constrain the deformation such that there is no interpenetration between the two surfaces. The normal stress field $S(x, y)$ that satisfies no penetration is obtained using an iterative method. The analytical solution for vertical/normal displacement due to a point force on an elastic half space is known as the Boussinesq solution, $B(r) = \frac{(1-\nu)}{2\pi G}\frac{1}{r}$, where G is the shear modulus and ν is the Poisson ratio. The normal displacement $w(x, y)$ due to the stress field $S(x, y)$ is obtained by convolution of the Boussinesq solution: $w(x,y) = \iint S(x',y')B(r)dx'dy'$, which takes into account the interactions between microcontacts. The solution is obtained via the two-dimensional FFT. We iteratively update $S(x, y)$ until the stress field satisfies the zero interpenetration condition [*Unger and Mase*, 1993]. In our simulations, we used $G = 10$ GPa and $\nu = 0.25$, which are realistic values for Berea sandstone under confining stress around 30 MPa [*Wang*, 2000]. By solving the elastic deformation problem for different values of $\bar{b}$, we obtain the

average normal stress $\bar{S}$ over the fracture surface for fixed $\bar{b}$, $\bar{S}=\iint S(x,y)dxdy/(LW)$, where L and W are the longitudinal and transverse dimensions of the fracture. Finally, we compute the fracture compliance as $C=d\bar{b}/d\bar{S}$.

Fracture compliance values have been estimated not only numerically but also in laboratory and field studies [Pyrak-Nolte and Morris, 2000; Zangerl et al., 2008; Hobday and Worthington, 2012].

A3. Estimation of Fracture Transmissivity

To obtain the fracture transmissivity, we perform a fluid flow simulation for incompressible fluid with constant viscosity on the final fracture geometry from the elastic deformation simulation, at each value of the mean fracture aperture $\bar{b}$. We take the aperture map $b(x, y)$ as the gap width in an equivalent parallel-plate model [*Moreno et al*., 1988]. By applying the lubrication approximation, we obtain a Darcy-type equation for the gap-averaged fluid velocity, $\mathbf{u}=-\frac{b^2}{12\mu}\nabla P$, where b is the local value of fracture aperture, μ is the dynamic viscosity of the fluid, and P is the fluid pressure. Conservation of mass imposes that the gap-integrated velocity, or volumetric flux, $\mathbf{q}=\mathbf{u}b$, be divergence-free: $\nabla\cdot\mathbf{q}=0$. We obtain the fluid pressure by solving the system of equations given by Darcy's law and mass conservation, with the following boundary conditions: constant pressure boundary condition at the left and right boundaries (P_L and P_R, respectively), and no-flow boundary condition at the top and bottom boundaries.

We obtain the cubic-law equivalent hydraulic aperture (h_c) for a stressed rough surface using the following relation: $Q_{\text{out}}=-\frac{h_c^3 W}{12\mu}\frac{P_R-P_L}{L}$, where $Q_{\text{out}}=\int_{\Gamma_{\text{out}}}\mathbf{q}\cdot\mathbf{n}\,d\Gamma$ is the total outflow, W is the width of the fracture surface (in the direction perpendicular to the flow) [*Tsang*, 1992]. The cubic-law equivalent aperture relates to the transmissivity of the fracture, $T=h_c^3/12$.

A4. Summary

In summary, the rock-physics model is a relationship between the fracture compliance C [m Pa^{-1}] and the fracture transmissivity T [m^2 s^{-1}] (Figure 3). Such relationship links the mechanical and hydraulic behaviors of a fracture, and constitutes the central element of our framework for sequential coupled flow-seismic inversion.

Appendix B: Double-Beam Inversion Method for Fracture Media

In this appendix, we give additional details on the seismic interpretation method we use—the double-beam method—and its application to the synthetic test case [*Zheng et al*., 2013].

B1. The Double-Beam Method

The double-beam method synthesizes a group of sources into a directional beam. The beam has a finite width and is shot into the subsurface to illuminate a specific small target region in the reservoir. The beam interacts with the fractures in the illuminated region and produces scattered beams (including multiply scattered waves among fractures in the local target region) that travel up to the Earth's surface. The scattered beam amplitude and direction are related to the fracture orientation, spacing and compliance. The same target region can be illuminated from different angles by multiple beams shot from the surface source locations. Collectively, the scattered beams in the recorded seismic data can be extracted to estimate local fracture parameters in that region. We then select the next target in the reservoir to repeat the procedure outlined above. In summary, the input to the double-beam method includes: (1) a macro seismic velocity model, which can be readily obtained by widely used methods such as the semblance velocity analysis; and (2) the surface recorded seismic waveforms. The output includes: fracture network geometry, fracture orientation, spacing between fractures, and the local fracture scattering coefficient (linearly proportional to the local fracture compliance field). All these parameters are a function of spatial location.

B2. Model Setup for the Synthetic Example

The seismic model for the synthetic example is a 3-D layered model (Figure 9). The third layer is the fractured reservoir, which contains two sets of mutually orthogonal fractures. The fracture planes are vertical and bounded by the reservoir layer thickness. We simulate seismic sources and geophones on the surface. The geophones record the fracture-scattered signal and reflections among layers (i.e., signal-generated noise). The layer boundaries can be constrained very effectively by conventional structural seismic imaging.

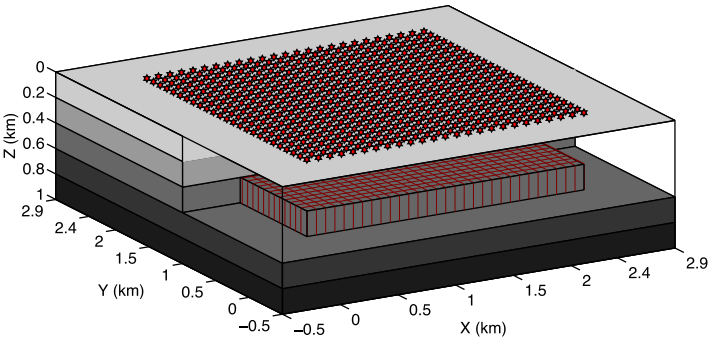

Figure 9. The 3-D view for the fractured reservoir model in a five-layer geological model. All layers have the same thickness, 200 m. The *P* wave velocities V_p in the layers are, in top-down order, 3.0, 3.2, 3.5, 3.8, and 4.0 km/s. The ratio between the *P* wave and the *S* wave velocities is $V_p/V_s = 1.7$. The medium densities for the layers are, from top to bottom, 2.20, 2.22, 2.25, 2.28, and 2.30 g/cm^3. The third layer is fractured within an area $0 \leq x \leq 2.4$ km and $0 \leq y \leq 2.4$ km. We use 2401 sources equidistantly located on the *x-y* plane $[0, 2.4]$ km $\times [0, 2.4]$ km, with spacing 50 m. The receivers cover a square region on the *x-y* plane: $[-0.5, 2.9]$ km $\times [-0.5, 2.9]$ km, with 10 m spacing. The seismic source wavelet is a Ricker wavelet of central frequency 40 Hz. To model 3-D seismic waves in this model, we use a finite difference scheme (see text). Reprinted from *Zheng et al.* [2013] with permission from the Society of Exploration Geophysicists.

Here the objective is to use the surface recorded seismic data set to infer fracture parameters in the reservoir layer, namely, how many sets of fractures are in the reservoir, their preferential orientation, the spacing between fractures, and the fracture compliance field, all as functions of spatial location.

B3. Seismic Inversion Results for the Synthetic Example

Our algorithm is target oriented. We can specify the target location where fracture parameters will be inferred by the double-beam method. At this target location, we exhaustively search all possible fracture spacing (between 40 and 120 m) and fracture orientation (between 0° and 180°), and infer the fracture-scattering coefficient. Only for those parameters corresponding to the true subsurface scenario will the scattering coefficient be large.

We identify the maximum scattering amplitude for each fracture set for all target locations, and select a point with large fracture seismic-wave scattering coefficient to determine fracture orientation and spacing. We can also include uncertainty in the orientation and spacing estimation process but we did not consider this in the current manuscript. It is apparent from the results that the fracture network consists of two sets of fractures orthogonal to each other, with a dominant fracture spacing (Figure 10).

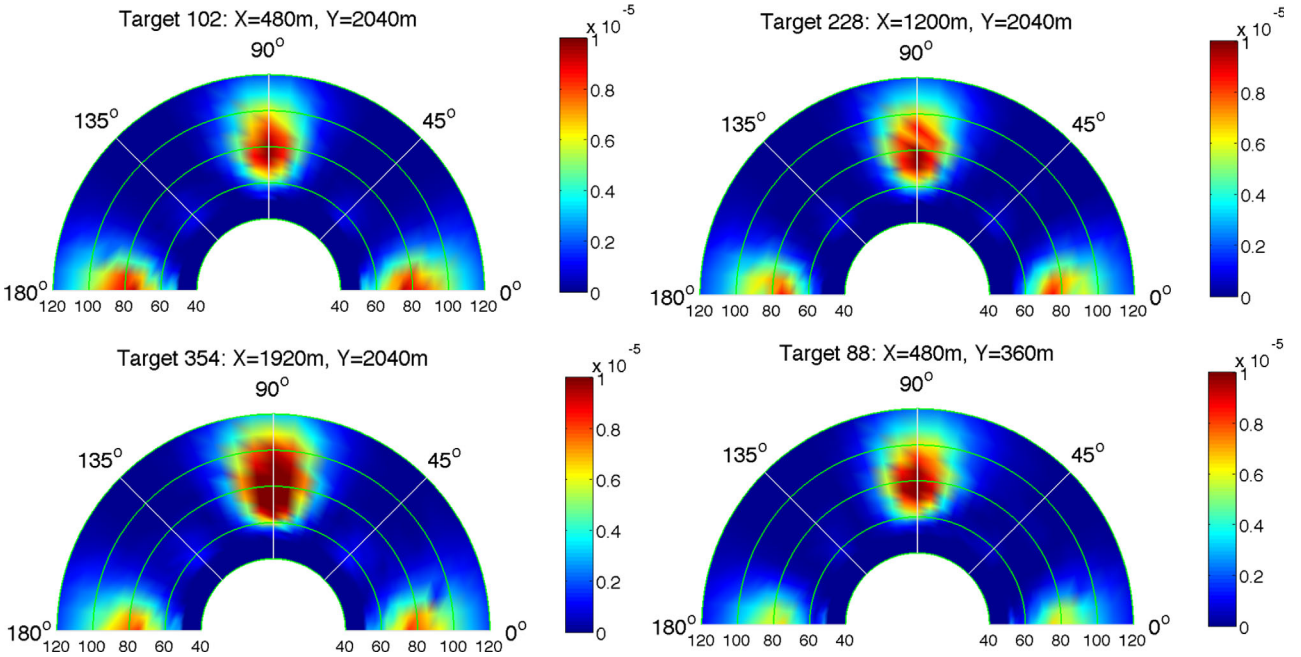

Figure 10. Fracture seismic-wave scattering coefficient for four targets in polar angle (fracture orientation) representation. The radius represents fracture spacing. The "bright spots" in these plots, corresponding to the highest values of scattering coefficient, accurately identify the true parameters of the fracture network in our model. It is evident that, for each target, there are two sets of fractures orthogonal to each other, with a dominant fracture spacing of 80 m. The bright spot at 180° and the 0° one indicate the same fracture plane (180° ambiguity for a plane). Reprinted from *Zheng et al.* [2013] with permission from the Society of Exploration Geophysicists.

We can plot the amplitudes in space and compare them with the true-model fracture compliance fields. Overall, the seismic amplitude and the fracture compliances show similar spatial patterns but, as expected, the values are not in the same range (Figures 5a and 5b). The double-beam method is not able to constrain the absolute values of fracture compliance but, as we show in this paper, this can be done by combining the seismic interpretation with hydrologic data.

Acknowledgments
This work was funded by Eni S.p.A. through the Multiscale Reservoir Science Project within the Eni-MIT Energy Initiative Founding Member Program. P.K.K. gratefully acknowledges support from the Korean Ministry of Land, Infrastructure and Transport (15AWMP-B066761-03). We thank the Society of Exploration Geophysicists to give us the permission to reprint the figures on the double-beam method (http://dx.doi.org/10.1190/geo2012-0512.1). The data to reproduce the work can be obtained from the corresponding author: Ruben Juanes (juanes@mit.edu).

References

Aarnes, J. E. (2004), On the use of a mixed multiscale finite element method for greater flexibility and increased speed or improved accuracy in reservoir simulation, *Multiscale Model. Simul.*, *2*(3), 421–439.
Aarnes, J. E., V. Kippe, and K.-A. Lie (2005), Mixed multiscale finite elements and streamline methods for reservoir simulation of large geomodels, *Adv. Water Resour.*, *28*, 257–271.
Andrews, D. J. (1988), On modeling closure of rough surfaces in contact, *Eos Trans. AGU*, *69*, 1426–1427.
Arbogast, T. (2002), Implementation of a locally conservative numerical subgrid upscaling scheme for two-phase Darcy flow, *Comput. Geosci.*, *6*(3–4), 453–481.
Bakku, S. K., M. Fehler, and D. Burns (2013), Fracture compliance estimation using borehole tube waves, *Geophysics*, *78*(4), D249–D260.
Bear, J., C. F. Tsang, and G. de Marsily (1993), *Flow and Contaminant Transport in Fractured Rock*, Academic, San Diego.
Brown, S. (1995), Simple mathematical model of a rough fracture, *J. Geophys. Res.*, *100*, 5941–5952.
Brown, S., and X. Fang (2012), Fluid flow property estimation from seismic scattering data, in *SEG Technical Program Expanded Abstracts*, pp. 1–6, Soc. of Explor. Geophys. [Available at http://library.seg.org/doi/pdfplus/10.1190/segam2012-1315.1.]
Brown, S., and C. H. Scholz (1985), Broad bandwidth study of the topography of natural rock surfaces, *J. Geophys. Res.*, *90*, 12,575–12,582.
Burns, D. R., M. E. Willis, M. N. Toksöz, and L. Vetri (2007), Fracture properties from seismic scattering, *Leading Edge*, *26*(9), 1186–1196.
Chen, J., S. Hubbard, J. Peterson, K. Williams, M. Fiene, P. Jardine, and D. Watson (2006), Development of a joint hydrogeophysical inversion approach and application to a contaminated fractured aquifer, *Water Resour. Res.*, *42*, W06425, doi:10.1029/2005WR004694.
Chen, Y., L. J. Durlofsky, M. Gerritsen, and X. H. Wen (2003), A coupled local–global upscaling approach for simulating flow in highly heterogeneous formations, *Adv. Water Resour.*, *26*(10), 1041–1060.
Coates, R. T., and M. Schoenberg (1995), Finite-difference modeling of faults and fractures, *Geophysics*, *60*, 1514–1526.
Copty, N., Y. Rubin, and G. Mavko (1993), Geophysical-hydrological identification of field permeabilities through Bayesian updating, *Water Resour. Res.*, *29*, 2813–2825.
Cueto-Felgueroso, L., and R. Juanes (2013), Forecasting long-term gas production from shale, *Proc. Natl. Acad. Sci. U. S. A.*, *110*(49), 19,660–19,661, doi:10.1073/pnas.1319578110.
Curtis, J. B. (2002), Fractured shale-gas systems, *AAPG Bull.*, *86*, 1921–1938.
Cvetkovic, V., S. Painter, N. Outters, and J. O. Selroos (2004), Stochastic simulation of radionuclide migration in discretely fractured rock near the Äspö Hard Rock Laboratory, *Water Resour. Res.*, *40*, W02404, doi:10.1029/2003WR002655.
Day-Lewis, F. D., K. Singha, and A. M. Binley (2005), Applying petrophysical models to radar travel time and electrical resistivity tomograms: Resolution-dependent limitations, *J. Geophys. Res.*, *110*, B08206, doi:10.1029/2004JB003569.
Dorn, C., N. Linde, T. Le Borgne, O. Bour, and M. Klepikova (2012), Inferring transport characteristics in a fractured rock aquifer by combining single-hole ground-penetrating radar reflection monitoring and tracer test data, *Water Resour. Res.*, *48*, W11521, doi:10.1029/2011WR011739.
Duguid, J. O., and P. C. Y. Lee (1977), Flow in fractured porous media, *Water Resour. Res.*, *13*, 558–566.
Durlofsky, L. J. (1991), Numerical calculation of equivalent grid block permeability tensors for heterogeneous porous media, *Water Resour. Res.*, *27*, 699–708.
Eberhart, R. C., and J. Kennedy (1995), A new optimizer using particle swarm theory, in *Proceedings of the Sixth International Symposium on Micro Machine and Human Science*, vol. 1, pp. 39–43, IEEE, N. Y.
Engelder, T. (2012), Capillary tension and imbibition sequester frack fluid in Marcellus gas shale, *Proc. Natl. Acad. Sci. U. S. A.*, *109*(52), E3625.
Fang, X., M. Fehler, T. Chen, D. Burns, and Z. Zhu (2013), Sensitivity analysis of fracture scattering, *Geophysics*, *78*, T1–T10.
Gabriel, K. J., and H. S. Colburn (1981), Interaural correlation discrimination: I. Bandwidth and level dependence, *J. Acoust. Soc. Am.*, *69*, 1394–1401.
Glover, P. W. J., K. Matsuki, R. Hikima, and K. Hayashi (1998), Synthetic rough fractures in rocks, *J. Geophys. Res.*, *103*, 9609–9620.
Goff, J. A. (1990), Comment on "Fractal mapping of digitized images: Application to the topography of Arizona and comparison with synthetic images" by J. Huang and D. L. Turcotte, *J. Geophys. Res.*, *95*, 5159–5159.
González, P. J., K. F. Tiampo, M. Palano, F. Cannavó, and J. Fernández (2012), The 2011 Lorca earthquake slip distribution controlled by groundwater crustal unloading, *Nat. Geosci.*, *5*(11), 821–825.
Grant, M. A., I. G. Donaldson, and P. F. Bixley (1983), *Geothermal Reservoir Engineering*, Academic Press, N. Y.
Hinnell, A. C., T. P. A. Ferré, J. A. Vrugt, J. A. Huisman, S. Moysey, J. Rings, and M. B. Kowalsky (2010), Improved extraction of hydrologic information from geophysical data through coupled hydrogeophysical inversion, *Water Resour. Res.*, *46*, W00D40, doi:10.1029/2008WR007060.
Hobday, C., and M. H. Worthington (2012), Field measurements of normal and shear fracture compliance, *Geophys. Prospect.*, *60*(3), 488–499.
Hooke, R., and T. A. Jeeves (1961), "Direct search" solution of numerical and statistical problems, *J. Assoc. Comput. Mach.*, *8*(2), 212–229.
Hubbard, S. S., and Y. Rubin (2000), Hydrogeological parameter estimation using geophysical data: a review of selected techniques, *J. Contam. Hydrol.*, *45*, 3–34.
Hyndman, D. W., J. M. Harris, and S. M. Gorelick (1994), Coupled seismic and tracer test inversion for aquifer property characterization, *Water Resour. Res.*, *30*, 1965–1977.
Hyndman, D. W., J. M. Harris, and S. M. Gorelick (2000), Inferring the relation between seismic slowness and hydraulic conductivity in heterogeneous aquifers, *Water Resour. Res.*, *36*, 2121–2132.
Irving, J., and K. Singha (2010), Stochastic inversion of tracer test and electrical geophysical data to estimate hydraulic conductivities, *Water Resour. Res.*, *46*, W11514, doi:10.1029/2009WR008340.

Jenny, P., S. H. Lee, and H. A. Tchelepi (2003), Multi-scale finite-volume method for elliptic problems in subsurface flow simulation, *J. Comput. Phys.*, *187*(1), 47–67.
Jha, B., and R. Juanes (2014), Coupled multiphase flow and poromechanics: A computational model of pore-pressure effects on fault slip and earthquake triggering, *Water Resour. Res.*, *50*, 3776–3808, doi:10.1002/2013WR015175.
Juanes, R., and F.-X. Dub (2008), A locally conservative variational multiscale method for the simulation of porous media flow with multiscale source terms, *Comput. Geosci.*, *12*(3), 273–295, doi:10.1007/s10596-007-9070-x.
Juanes, R., and H. A. Tchelepi (2008), Special issue on multiscale methods for flow and transport in heterogeneous porous media, *Comput. Geosci.*, *12*(3), 255–256, doi:10.1007/s10596-008-9084-z.
Kang, P. K., M. Dentz, T. Le Borgne, and R. Juanes (2011), Spatial Markov model of anomalous transport through random lattice networks, *Phys. Rev. Lett.*, *107*, 180602, doi:10.1103/PhysRevLett.107.180602.
Kang, P. K., T. Le Borgne, M. Dentz, O. Bour, and R. Juanes (2015a), Impact of velocity correlation and distribution on transport in fractured media: field evidence and theoretical model, *Water Resour. Res.*, *51*, 940–959, doi:10.1002/2014WR015799.
Kang, P. K., M. Dentz, T. Le Borgne, and R. Juanes (2015b), Anomalous transport on regular fracture networks: Impact of conductivity heterogeneity and mixing at fracture intersections, *Phys. Rev. E*, *92*(2), 022148.
Kazemi, H., and J. R. Gilman (1993), *Multiphase Flows in Fractured Petroleum Reservoirs*, Academic, N. Y.
Kippe, V., J. E. Aarnes, and K.-A. Lie (2008), A comparison of multiscale methods for elliptic problems in porous media flow, *Comput. Geosci.*, *12*(3), 377–398, doi:10.1007/s10596-007-9074-6./.
Kiraly, L. (1979), Remarques sur la simulation des failles et du réseau karstique par éléments finis dans les modèles d'écoulement, *Bull. Cent. Hydrogéol.*, *3*, 155–167.
Kiraly, L. (1987), Large scale 3-D groundwater flow modeling in highly heterogeneous geologic medium, in *Groundwater Flow and Quality Modeling*, edited by E. Custodio et al., pp. 761–775, D. Reidel, Dordrecht, Netherlands.
Kool, J. B., and J. C. Parker (1988), Analysis of the inverse problem for transient unsaturated flow, *Water Resour. Res.*, *24*, 817–830.
Le Borgne, T., O. Bour, F. L. Paillet, and J.-P. Caudal (2006), Assessment of preferential flow path connectivity and hydraulic properties at single-borehole and cross-borehole scales in a fractured aquifer, *J. Hydrol.*, *328*, 347–359.
Lee, H. S., and T. F. Cho (2002), Hydraulic characteristics of rough fractures in linear flow under normal and shear load, *Rock Mech. Rock Eng.*, *35*(4), 299–312.
Linde, N., S. Finsterle, and S. Hubbard (2006), Inversion of tracer test data using tomographic constraints, *Water Resour. Res.*, *42*, W04410, doi:10.1029/2004WR003806.
Lochbühler, T., J. Doetsch, R. Brauchler, and N. Linde (2013), Structure-coupled joint inversion of geophysical and hydrological data, *Geophysics*, *78*(3), ID1–ID14.
Martinez-Landa, L., J. Carrera, M. Dentz, D. Fernandez-Garcia, A. Nardi, and M. W. Saaltink (2012), Mixing induced reactive transport in fractured crystalline rocks, *Appl. Geochem.*, *27*(2), 479–489.
McKenna, S. A., and E. P. Poeter (1995), Field example of data fusion in site characterization, *Water Resour. Res.*, *31*, 3229–3240.
Menke, W. (2012), *Geophysical Data Analysis: Discrete Inverse Theory*, Academic.
Molinero, J., J. Samper, and R. Juanes (2002), Numerical modeling of the transient hydrogeological response produced by tunnel construction in fractured bedrocks, *Eng. Geol.*, *64*(4), 369–386.
Moreno, L., and I. Neretnieks (1993), Fluid flow and solute transport in a network of channels, *J. Contam. Hydrol.*, *14*, 163–194.
Moreno, L., Y. W. Tsang, C. F. Tsang, F. V. Hale, and I. Neretnieks (1988), Flow and tracer transport in a single fracture: A stochastic model and its relation to some field observations, *Water Resour. Res.*, *24*, 2033–2048.
Nogi, T., and T. Kato (1997), Influence of a hard surface layer on the limit of elastic contact. Part I: Analysis using a real surface model, *J. Tribol.*, *119*(3), 493–500.
Ogilvie, S. R., E. Isakov, and P. W. J. Glover (2006), Fluid flow through rough fractures in rocks. II: A new matching model for rough rock fractures, *Earth Planet. Sci. Lett.*, *241*(3), 454–465.
Petrovitch, C. L., L. J. Pyrak-Nolte, and D. D. Nolte (2013), Scaling of fluid flow versus fracture stiffness, *Geophys. Res. Lett.*, *40*, 2076–2080, doi:10.1002/grl.50479.
Polonsky, I. A., and L. M. Keer (1999), A numerical method for solving rough contact problems based on the multi-level multi-summation and conjugate gradient techniques, *Wear*, *231*(2), 206–219.
Power, W. L., and T. E. Tullis (1991), Euclidean and fractal models for the description of rock surface roughness, *J. Geophys. Res.*, *96*, 415–424.
Pruess, K., J. S. Y. Wang, and Y. W. Tsang (1990), On thermohydrologic conditions near high-level nuclear wastes emplaced in partially saturated fractured tuff: 1. Simulation studies with explicit consideration of fracture effects, *Water Resour. Res.*, *26*, 1235–1248.
Pyrak-Nolte, L. J., and J. P. Morris (2000), Single fractures under normal stress: The relation between fracture specific stiffness and fluid flow, *Int. J. Rock Mech. Min. Sci.*, *37*, 245–262.
Rubin, Y., G. Mavko, and J. Harris (1992), Mapping permeability in heterogeneous aquifers using hydrologic and seismic data, *Water Resour. Res.*, *28*, 1809–1816.
Sayers, C. M., and L. D. den Boer (2012), Characterizing production-induced anisotropy of fractured reservoirs having multiple fracture sets, *Geophys. Prospect.*, *60*(5), 919–939.
Schoenberg, M. (1980), Elastic wave behavior across linear slip interfaces, *J. Acoust. Soc. Am.*, *68*, 1516–1521.
Shi, Y., and R. Eberhart (1998), A modified particle swarm optimizer, in *Evolutionary Computation Proceedings*, pp. 69–73, IEEE.
Tsang, Y. W. (1992), Usage of "equivalent apertures" for rock fractures as derived from hydraulic and tracer tests, *Water Resour. Res.*, *28*, 1451–1455.
Unger, A. J. A., and C. W. Mase (1993), Numerical study of the hydromechanical behavior of two rough fracture surfaces in contact, *Water Resour. Res.*, *29*, 2101–2114.
Vlastos, S., E. Liu, I. G. Main, M. Schoenberg, C. Narteau, X. Y. Li, and B. Maillot (2006), Dual simulations of fluid flow and seismic wave propagation in a fractured network: Effects of pore pressure on seismic signature, *Geophys. J. Int.*, *166*, 825–838.
Walsh, R., C. McDermott, and O. Kolditz (2008), Numerical modeling of stress-permeability coupling in rough fractures, *Hydrogeol. J.*, *16*(4), 613–627.
Wang, H. F. (2000), *Theory of Linear Poroelasticity*, Princeton Univ. Press, Princeton, N. J.
Warner, N. R., R. B. Jackson, T. H. Darrah, S. G. Osborn, A. Down, K. Zhao, A. White, and A. Vengosh (2012), Geochemical evidence for possible natural migration of Marcellus Formation brine to shallow aquifers in Pennsylvania, *Proc. Natl. Acad. Sci. U. S. A.*, *109*(30), 11,961–11,966.

Willis, M. E., D. R. Burns, R. Rao, B. Minsley, M. N. Toksöz, and V. L. (2006), Spatial orientation and distribution of reservoir fractures from scattered seismic energy, *Geophysics*, *71*, O43–O51.

Worthington, M. H., and R. Lubbe (2007), The scaling of fracture compliance, *Geol. Soc. Spec. Publ.*, *270*, 73–82.

Yadav, G. S., and S. K. Singh (2007), Integrated resistivity surveys for delineation of fractures for ground water exploration in hard rock areas, *J. Appl. Geophys.*, *62*(3), 301–312.

Zangerl, C., K. F. Evans, E. Eberhardt, and S. Loew (2008), Normal stiffness of fractures in granitic rock: A compilation of laboratory and in-situ experiments, *Int. J. Rock Mech. Min. Sci.*, *45*(8), 1500–1507.

Zhang, Y., C. M. Sayers, and J. I. Adachi (2009), The use of effective medium theories for seismic wave propagation and fluid flow in fractured reservoirs under applied stress, *Geophys. J. Int.*, *177*, 205–221.

Zheng, Y., X. Fang, M. C. Fehler, and D. R. Burns (2013), Seismic characterization of fractured reservoirs by focusing Gaussian beams, *Geophysics*, *78*, A23–A28.